catalysts

MDPI

Communication

Selective Catalytic Transfer Hydrogenolysis of Glycerol to 2-Isopropoxy-Propan-1-Ol over Noble Metal Ion-Exchanged Mordenite Zeolite

Bhupendra Kumar Singh, Yongseok Kim, Seungdon Kwon and Kyungsu Na *

Department of Chemistry, Chonnam National University, 77 Yongbong-ro, Buk-gu, Gwangju 61186, Korea; bkchauhan2004@gmail.com (B.K.S.); sandarayong@gmail.com (Y.K.); kwon950515@gmail.com (S.K.)
* Correspondence: kyungsu_na@chonnam.ac.kr; Tel.: +82-62-530-3494

Received: 9 October 2019; Accepted: 24 October 2019; Published: 25 October 2019

Abstract: This study investigated the selective conversion of glycerol to 2-isopropoxy-propan-1-ol over noble metal ion-exchanged mordenite zeolites (RuMOR, RhMOR, and PdMOR) as heterogeneous catalysts via catalytic transfer hydrogenolysis (CTH) using propan-2-ol as the solvent, hydrogen supplier, and reactive coupling reagent with glycerol. The catalytic reactions were performed at 140 °C under inert conditions with a 0.5 MPa initial pressure of N_2. A single product, 2-isopropoxy-propan-1-ol, was catalytically generated without any appreciable by-products. The catalytic results were reproducible, and the catalysts exhibited good recyclability.

Keywords: mordenite zeolite; catalytic transfer hydrogenolysis; 2-isopropoxy-propan-1-ol; glycerol; noble metal

1. Introduction

The use of renewable biomass resources for various chemical production processes provides an avenue for chemical industries to reduce their sole dependence on waning fossil-based resources and to alleviate CO_2 emissions [1]. The production of sustainable fuel and chemicals from biomass feedstocks is an attractive approach compared to the use of conventional petroleum-based fuel and chemicals [2]. Biodiesel production through transesterification of vegetable oils cogenerates glycerol on a large scale (~10%). The global production of glycerol is expected to reach 6 million tons by 2025 [3]. Glycerol is currently considered as one of the most promising platform chemicals because of its non-toxic and biodegradable properties [4]. The high demand for and production of biodiesel has resulted in an oversupply of glycerol, consequently reducing the average price in the current chemical market [5]. The efficient conversion of glycerol to several value-added chemicals and fuels has been achieved via various highly applicable catalytic reactions, including oxidation, hydrogenolysis, dehydration, acetalization, and esterification [6–8].

Among the aforementioned reactions, hydrogenolysis of glycerol is a useful route for the production of important chemicals such as propane-1,3-diol, propane-1,2-diol, and ethylene glycol, which are commonly utilized in the synthesis of various valuable products, including pharmaceuticals, cosmetics, flavors, fragrances, and antifreezes [9,10]. Various noble and non-noble metals, including Pt, Rh, Ru, Pd, Cu, and Ni, supported on catalytic materials have been widely applied in common hydrogenolysis reactions as they are highly efficient for cleaving the various bonds in the glycerol molecule [11–14]. The use of bimetallic catalysts over a wide range of reaction temperatures and pressures has also been reported [15,16]. To ensure experimental safety and tempered energy consumption, employing low pressure and avoiding the use of external hydrogen are recommended [17,18]. Previous studies also proved that during hydrogenolysis of glycerol, the solvent itself (e.g., ethanol or propan-2-ol)

could produce the necessary hydrogen for the reaction. This methodology is termed catalytic transfer hydrogenolysis (CTH), which provides a facile approach for the hydrogenolysis of glycerol to various value-added products [19].

Herein, we report a new approach for the efficient conversion of glycerol to 2-isopropoxy-propan-1-ol over various noble metal ion-exchanged mordenite (MOR) zeolite catalysts (RuMOR, PdMOR, and RhMOR) in the absence of external H_2 via the CTH reaction, where propan-2-ol is used not only as the solvent but also as the hydrogen supplier and glycerol coupling reagent for the production of 2-isopropoxy-propan-1-ol (Figure S1; Supplementary Materials). MOR zeolite is synthesized via a hydrothermal method, and the noble metals are introduced into the zeolite framework by ion-exchange with the chloride salts of Ru, Rh, and Pd. These catalysts are characterized by powder X-ray diffraction (XRD), scanning electron microscopy (SEM), transmission electron microscopy (TEM), X-ray photoelectron spectroscopy (XPS), thermogravimetric analysis (TGA), solid-state magic angle spinning (MAS) ^{27}Al nuclear magnetic resonance (NMR), N_2 adsorption isotherm, and inductively coupled plasma-optical emission spectrometry (ICP-OES).

2. Results and Discussion

2.1. Characterization of the Catalysts

2.1.1. XRD and SEM Analysis

Figure 1a shows the wide-angle powder XRD patterns of MOR zeolite and the series of noble metal ion-exchanged zeolites. The XRD patterns of as-synthesized NaMOR zeolite (i.e., NaMOR(as-syn)) and the corresponding calcined sample (i.e., NaMOR(cal)) showed the XRD reflections of the fully crystalline MOR framework (JCPDS no. 29-1257) [20]. The XRD patterns of all the noble metal ion-exchanged MOR zeolites (i.e., XMOR(ion-ex) where X is Ru, Pd, or Rh) and the corresponding calcined samples showed that the pristine structure of the MOR framework remained intact after the introduction of various noble metals and subsequent calcination. No new XRD peaks originating from the noble metals were observed, proposing the very small particle size of the noble metals introduced into the MOR zeolites. Figure 1b–e present the SEM images of the calcined MOR zeolite samples (i.e., NaMOR(cal), RuMOR(cal), PdMOR(cal), and RhMOR(cal)), illustrating the micron-scale bulk crystalline morphology. There were no remarkable differences in the SEM images of the samples before and after ion-exchange with the noble metals and subsequent calcination. In addition, no appreciable amorphous phase was observed.

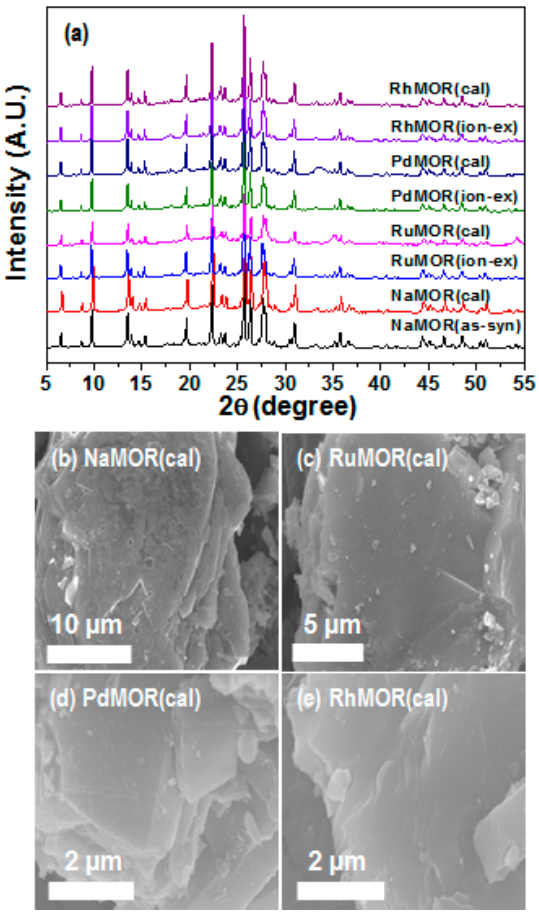

Figure 1. (**a**) X-ray diffraction (XRD) patterns of as-synthesized metal ion-exchanged mordenite (MOR) zeolite in the Na^+-form (NaMOR(as-syn)), its calcined form (NaMOR(cal)), noble metal ion-exchanged MOR zeolites (XMOR(ion-ex), where X is Ru, Pd or Rh) and their calcined forms (XMOR(cal)). (**b**–**e**) SEM images of calcined MOR zeolite samples (NaMOR(cal), RuMOR(cal), PdMOR(cal) and RhMOR(cal).

2.1.2. TEM and EDX Analysis

Figure 2(a–d)$_{i}$ present the TEM images of the calcined samples and the corresponding selected area electron diffraction (SAED) patterns (inset), confirming the bulk crystalline morphology of various MOR zeolite materials. Figure 2(a–d)$_{ii}$ present the high-angle annular dark-field scanning transmission electron microscopy (HAADF-STEM) images. Energy-dispersive X-ray spectroscopy (EDX) elemental mapping was used to identify the location (occupancy) of the elements (Si, Al, O, Na, Ru, Pd, and Ru) in the zeolite samples. Figure 2(a–d)$_{iii}$, (a–d)$_{iv}$, and (a–d)$_{v}$ show the elemental mapping of Si, O, and Al, respectively, confirming the uniform distribution of all the zeolite framework elements throughout the samples. Similarly, the elemental mapping images of Na, Ru, Pd, and Rh are shown in Figure 2(a–d)$_{vi}$. The ambiguous elemental mapping in Figure 2(a–d)$_{vi}$ is possibly due to the low content of these elements in the catalysts. Some amount of the noble metals was localized at the periphery of the zeolite crystals. However, highly dispersed noble metal atoms were also observed. Isothermal N_2 adsorption analysis was used to assess the Brunauer-Emmett-Teller (BET) surface area (S_{BET}) of the zeolite samples (Table S1; Supplementary Materials).

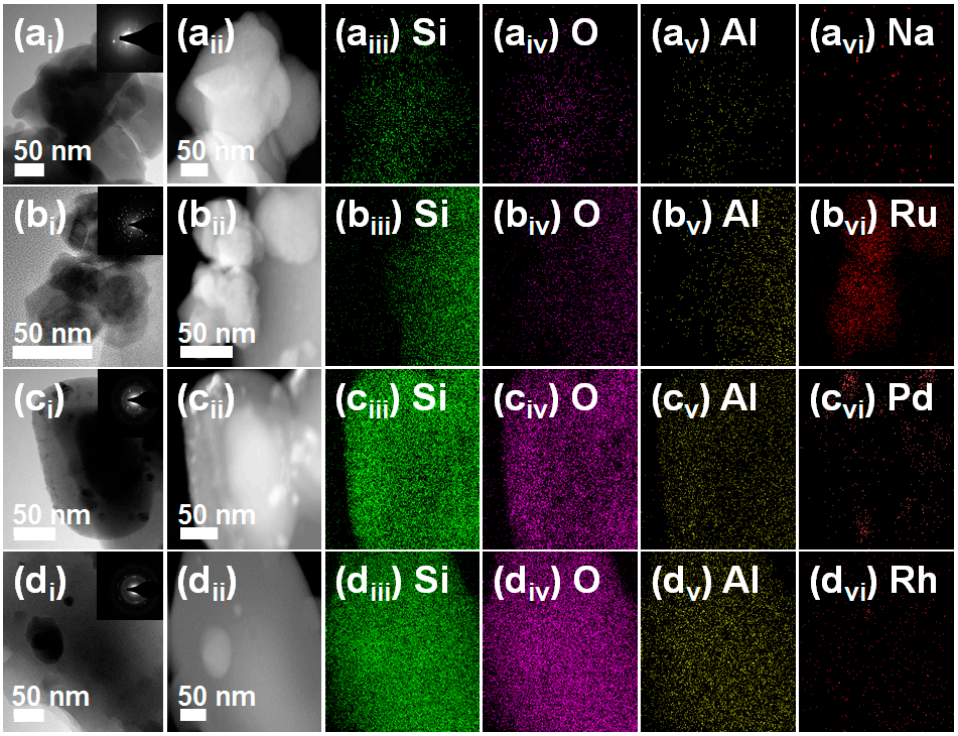

Figure 2. (**a**–**d**)$_{\mathbf{i}}$ Transmission electron microscopy (TEM) images of NaMOR(cal), RuMOR(cal), PdMOR(cal) and RhMOR(cal), respectively, and their high-angle annular dark-field scanning transmission electron microscopy (HAADF-STEM) images ((**a**–**d**)$_{\mathbf{ii}}$) with corresponding selected area electron diffraction (SAED) patterns (inset). EDX elemental mapping images for (**a**–**d**)$_{\mathbf{iii}}$ Si, (**a**–**d**)$_{\mathbf{iv}}$ O and (**a**–**d**)$_{\mathbf{v}}$ Al. EDX elemental mapping images in (**a**–**d**)$_{\mathbf{vi}}$ correspond to Na, Ru, Pd, and Rh in NaMOR(cal), RuMOR(cal), PdMOR(cal), and RhMOR(cal) samples, respectively.

2.1.3. XPS Analysis

XPS analysis was performed to determine the chemical and electronic state of Ru, Pd, and Rh species in the MOR zeolite samples. Figure 3a shows the full scan survey spectra of RuMOR(cal), PdMOR(cal), and RhMOR(cal), confirming the existence of Ru, Pd, and Rh in the respective RuMOR (~280.0–286.0 eV), PdMOR (~334.0–345.0 eV), and RhMOR (~307.0–31.05 eV) catalysts [21]. Figure 3b–m present the deconvoluted and fitted Ru3d, Pd3d, and Rh3d XPS spectra, along with the O1s, Si2p, and Al2p XPS spectra. The fitted Ru3d spectra are shown in Figure 3b. Deconvolution of the Ru3d curve of RuMOR revealed three binding energy peaks at 280.5 eV (assigned to $Ru3d_{5/2}$), 282.1 eV (assigned to $Ru3d_{5/2}$), and 284.8 eV (assigned to $Ru3d_{3/2}$), which were related to the presence of Ru(0), RuO_2, and Ru(0), species, respectively [22,23]. The XPS data indicated that a few Ru species in RuMOR(cal) were partially reduced to form Ru(0) nanoparticles supported on MOR. Moreover, the $Ru3d_{3/2}$ line was expected to fall in the binding energy range of 284.1 to 284.2 eV, which was very close to the previous observation (at 284.6 eV) [24]. The peak at 282.1 eV was assigned to the RuO_2 species corresponding to the Ru(VI) oxidation state, which was formed by oxidation upon exposure of RuMOR(cal) to air [25]. The Pd3d spectra of PdMOR(cal) are shown in Figure 3c.

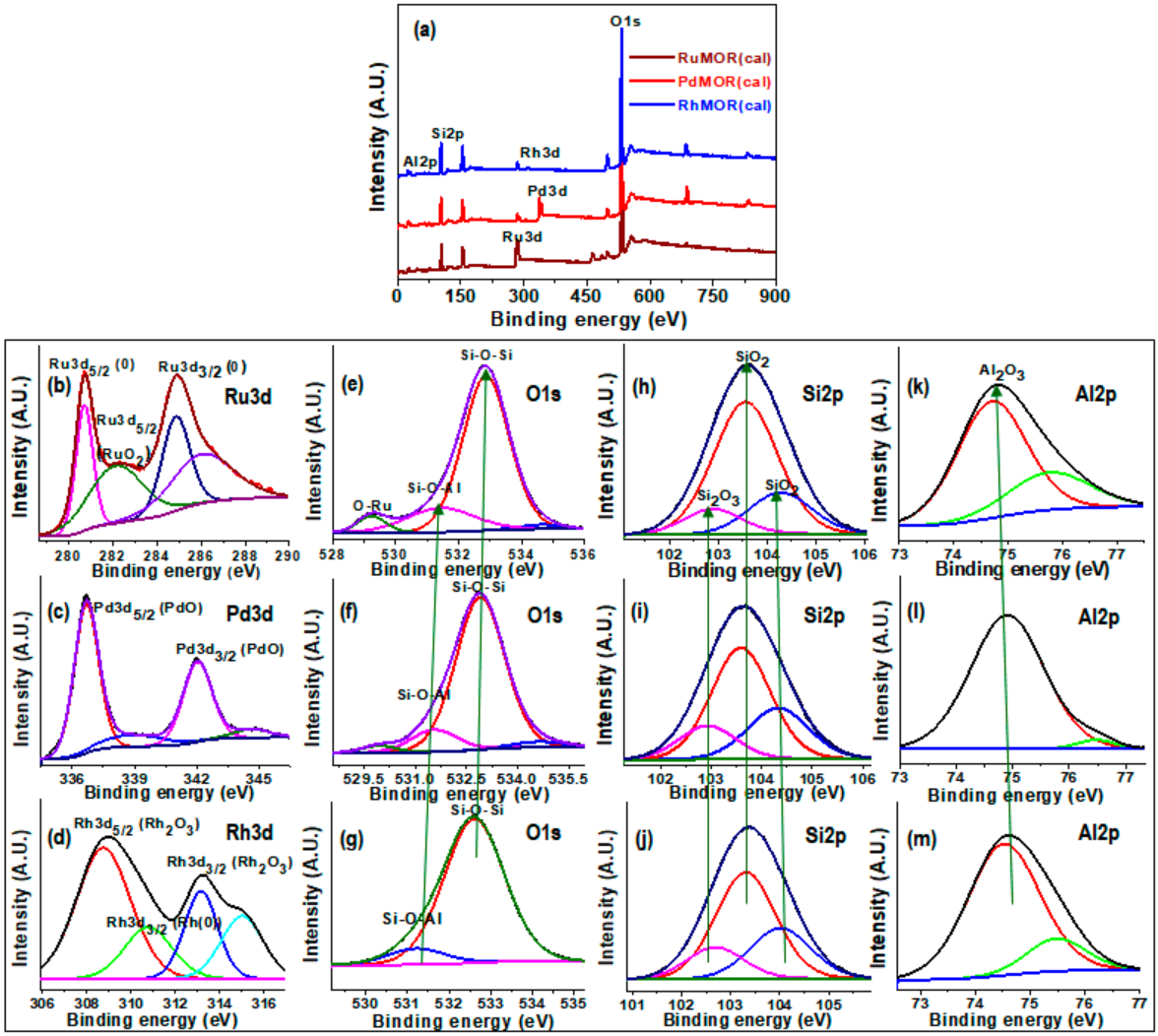

Figure 3. (**a**) Full scan survey X-ray photoelectron spectroscopy (XPS) spectra of calcined RuMOR(cal), PdMOR(cal), and RhMOR(cal) materials, confirming the existence of Ru in RuMOR (~280.0–286.0 eV), Pd in PdMOR (~334.0–345.0 eV), and Rh in RhMOR (~307.0–315.0 eV) along with the presence of O, Si, and Al chemical species. (**b**–**m**) Deconvoluted and fitted XPS spectra for Ru3d, Pd3d, Rh3d, O1s, Si2p, and Al2p in different chemical and electronic states.

The deconvoluted Pd3d spectra of PdMOR(cal) showed two peaks at 336.7 eV (assigned to $Pd3d_{5/2}$) and 342.1 eV (assigned to $Pd3d_{3/2}$), both of which were correlated to the PdO (Pd^{2+}) state [26]. The Rh3d signal for RhMOR(cal) (Figure 3d) was fitted to two discernible doublets with different intensities. The doublet observed at ~313.0 eV (assigned to $Rh3d_{3/2}$) and ~309.0 eV (assigned to $Rh3d_{5/2}$) was attributed to Rh_2O_3 [27]. The additional binding energy peak at 310.8 eV (assigned to $Rh3d_{3/2}$) was related to the presence of the Rh(0) NPs in the RhMOR sample [28]. The O1s spectra of all three samples (RuMOR, PdMOR, and RhMOR) are presented in Figure 3e–g). The major peak at 532.8 eV and a smaller peak at ~531.4 eV can be assigned to Si–O–Si and Si–O–Al linkages, respectively. The shoulder peak at 529.3 eV was assigned to the chemisorbed oxygen (O–Ru) in the RuMOR catalyst [29]. Figure 3h–j present the Si2p spectra for all catalysts. The major binding energy peak at 103.5 eV and the relatively smaller peak at 104.2 eV indicated the presence of the SiO_2 (Si^{4+} state). The peak at 102.8 eV corresponded to the Si_2O_3 species. The major peak at 74.8 eV in the Al2p spectrum confirmed the presence of the Al_2O_3 species (Figure 3k–m).

2.1.4. TGA and Solid-State MAS ^{27}Al NMR Spectroscopy

Figure 4a shows the TGA data for the NaMOR(cal), RuMOR(cal), PdMOR(cal), and RhMOR(cal) catalysts. A total weight loss of ~9% was observed over different temperature ranges, i.e., from 50 to 300 °C and thereafter up from 300 to 600 °C and beyond. The rapid weight loss in the temperature range of 50 to 300 °C was attributed to the desorption of water molecules present in the MOR zeolites. The weight loss in the temperature range of 300 to 600 °C with respect to RuMOR(cal), RhMOR(cal), and PdMOR(cal) could be ascribed in terms of the amount of Ru, Rh, and Pd present in these catalysts. It has been proven that the considerable weight loss in the metal-exchanged MOR zeolites (in this temperature range) increases with the amount of metal exchanged [30]. Our study firmly corroborates similar trends. Table S1 (ICP-OES data) presents the quantitative analysis (chemical composition) of the noble metal ion-exchanged MOR zeolites. The amount of Ru, Rh, and Pd in the ion-exchanged MOR is in 1:2.1:3.7 ratio. Therefore, the weight-loss trend (Figure 4a) obtained was PdMOR > RhMOR > RuMOR, which was attributed to the dehydroxylation from the hydroxylated noble metal species. These results indicate that all the materials are quite stable at high temperatures and that the stability of NaMOR(as-syn) was sustained after the addition of the noble metals. To understand the coordination of Al species within the MOR framework, all the samples (NaMOR(cal), RuMOR(cal), PdMOR(cal), and RhMOR(cal)) were characterized by solid-state MAS ^{27}Al NMR spectroscopy.

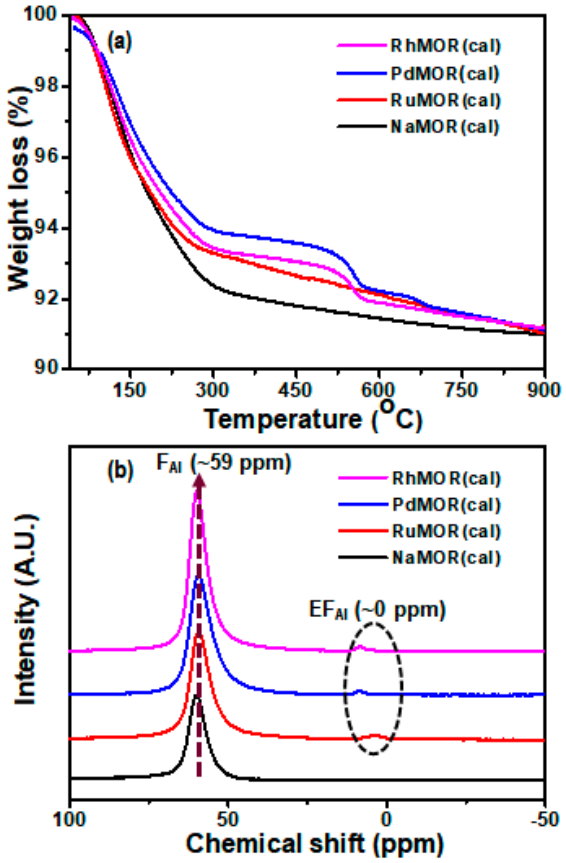

Figure 4. (**a**) Thermogravimetric analysis (TGA) data of NaMOR(cal), RuMOR(cal), PdMOR(cal), and RhMOR(cal), reflecting a total weight loss of ~9%. (**b**) Solid-state MAS ^{27}Al NMR spectra of NaMOR(cal), RuMOR(cal), PdMOR(cal), and RhMOR(cal). The strong peak at ~59 ppm is attributed to tetrahedrally coordinated framework aluminum atoms (F_{Al}). The low-intensity peak close to 0 ppm for RuMOR(cal), PdMOR(cal), and RhMOR(cal) correspond to the octahedrally coordinated extra-framework aluminum atoms (EF_{Al}).

Figure 4b presents the solid-state MAS ^{27}Al NMR spectra of all the samples. The most intense peak at ~59 ppm confirms the presence of tetrahedrally coordinated framework aluminum atoms (F_{Al}). A very low-intensity peak was also observed at ~0 ppm for the RuMOR(cal), PdMOR(cal), and RhMOR(cal) samples, which was attributed to the octahedrally coordinated extra-framework Al atoms (EF_{Al}) [31]. This analysis indicates that Al atoms in the MOR frameworks of NaMOR(cal), RuMOR(cal), PdMOR(cal), and RhMOR(cal) are mainly arranged as tetrahedrally coordinated F_{Al}, which further corroborates synthesis of the highly stable MOR catalysts.

2.2. Catalytic Transfer Hydrogenolysis of Glycerol

All four materials (NaMOR(cal), RuMOR(cal), PdMOR(cal), and RhMOR(cal)) were applied in the CTH conversion of glycerol to 2-isopropoxy-propan-1-ol, a highly applicable solvent for resin, dyes, and surface coatings [32,33]. A series of experiments were conducted under different conditions with variation in reaction time (24, 48, 72, and 96 h) and temperature (120, 140, and 160 °C). Prior to the reactions, the system was purged with N_2 gas and 0.5 MPa was used as the initial reactor pressure for all experiments (the reactor pressure was 1.4 MPa under the optimized reaction conditions (at 140 °C and 500 rpm for 72 h)). The experimental parameters had a major impact on the reaction efficiency, and most importantly, on the product selectivity. The products were identified by gas chromatography mass spectrometry (GCMS) and proton NMR analysis (Figures S2 and S3; Supplementary Materials). The strong peak at m/z 117 (M-1 peak) corroborated the conversion of glycerol to 2-isopropoxy-propan-1-ol (Figure S2), and the ^{1}H NMR spectra after CTH conversion of glycerol in the presence of propan-2-ol showed the chemical shifts of 2-isopropoxy-propan-1-ol. The analyzed compound also contained residual glycerol and propan-2-ol, and, therefore, the signature peaks of propan-1-ol were merged with the product peaks (peaks a and b); the peaks of unutilized glycerol may also overlap with peaks c, d, and e (Figure S3). In order to confirm the product formation, we also analyzed the ^{1}H NMR spectra of the starting reaction mixture (glycerol and propan-2-ol in deuterated methanol, shown in Figure S4). The results clearly show differences in the intensity of the proton peaks at the corresponding chemical shifts.

A comparative analysis of the results obtained with the fresh (first run) and recycled (second run) catalysts for CTH conversion of glycerol is presented in Figure 5. The data represent the optimized results for the conversion of glycerol over all the catalysts. The catalytic efficiency (in terms of % conversion) in the first and second reaction runs with the catalysts is represented by red and blue lines, respectively. Interestingly, this reaction resulted in 100% product selectivity (2-isopropoxy-propan-1-ol), as only one additional peak in the GC and GCMS profiles of the solution after reaction was observed. The catalytic efficiency of fresh NaMOR(cal), RuMOR(cal), PdMOR(cal), and RhMOR(cal) was 22.3%, 69.7%, 26.9%, and 50.9%, respectively, for the reaction at 140 °C for 72 h (see the results for the first run catalysts). The catalytic performance changed slightly for all the recycled catalysts (see the results for the second run catalysts). The glycerol conversion achieved with the spent catalysts was 20.1%, 62.9%, 22.1%, and 46.7%, respectively, for NaMOR(cal), RuMOR(cal), PdMOR(cal), and RhMOR(cal). The enhanced catalytic performance of the RuMOR(cal) and RhMOR(cal) catalysts relative to that of PdMOR(cal) was attributed to the strong coordination of Ru and Rh with MOR (due to the +3 oxidation state of Ru and Rh, whereas Pd remains in the divalent state in PdMOR(cal)). The highest catalytic efficiency exhibited by the RuMOR(cal) catalyst can be correlated to the XPS data, which indicates the presence of chemisorbed oxygen (O–Ru) with a binding energy of 529.3 eV [29]. The chemisorbed oxygen would lead to strong interaction between MOR and Ru metal, thereby augmenting the stability of the catalyst. Moreover, the impact of the larger surface area could also be a key factor contributing to the superior catalytic performance of RuMOR.

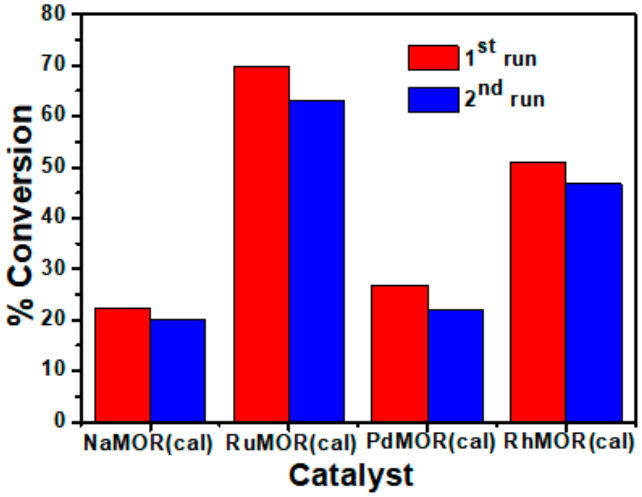

Figure 5. Catalytic performance of fresh (1st run) and recycled (2nd run) NaMOR(cal), RuMOR(cal), PdMOR(cal), and RhMOR(cal) materials for catalytic transfer hydrogenolysis (CTH) conversion of glycerol to 2-isopropoxy-propan-1-ol. The reaction was performed in a batch reactor at 140 °C for 72 h under an inert atmosphere, and at 0.5 MPa initial N_2 pressure (the autogenous pressure was 1.4 MPa during the reaction). RuMOR(cal) catalyst was found to be most efficient for conversion, which is attributed to the strong interaction between Ru and MOR, as evident from the XPS data (indicated by the binding energy peak of chemisorbed Ru-O at 529.3 eV).

3. Materials and Methods

3.1. Materials

All chemicals used for the study were of analytical reagent grade (from Sigma-Aldrich (MO, USA), TCI (Tokyo, Japan), and Daejung chemicals (Gyeonggi-do, Korea), and were used without further purification. $NaAlO_2$, Ludox silica (30 wt.%), $RuCl_3$, $PdCl_2$, and glycerol were purchased from Sigma-Aldrich (MO, USA). NaOH, isopropyl alcohol, and $RhCl_3{\cdot}_X H_2O$ were obtained from Daejung chemicals (Gyeonggi-do, Korea), and dodecane was purchased from TCI chemicals (Tokyo, Japan). Deionized water with a specific resistivity of 16.82 MΩ cm at 25 °C was prepared with a commercial deionizer (Seoul, Korea).

3.2. Methods

3.2.1. Synthesis of Mordenite (MOR)

In a typical synthesis, 0.40 g NaOH was placed into 14 g of deionized water and stirred for 15 min to form a transparent solution. To this solution, 0.2 g of $NaAlO_2$ was added, stirred for another 15 min, and 6 g Ludox silica (30 wt.% aqueous solution) was further added to the solution. The resultant gel comprising 29.96 SiO_2:5.97 Na_2O:1.22 Al_2O_3:777.78 H_2O was stirred for 2 h at ambient temperature. The final gel was transferred to a Teflon-lined stainless-steel autoclave and kept in an oven for crystallization at 180 °C for 48 h at a tumbling rate of 25 rpm. After the synthesis, the autoclave was cooled in water, and the product was filtered, washed with deionized water, and dried at 100 °C overnight. The obtained powder was further calcined in air at 450 °C for 4 h. The synthesized mordenite powder was denoted as NaMOR(as-syn) and NaMOR(cal) before and after calcination, respectively.

3.2.2. Synthesis of Noble Metal Ion-Exchanged Mordenites (RuMOR, RhMOR, and PdMOR)

RuMOR, RhMOR, and PdMOR catalysts were synthesized via ion-exchange using $RuCl_3$ (Ru content: 45%–55% by weight), $RhCl_3{\cdot}xH_2O$ (Rh content: ~40% by weight), and $PdCl_2$ (Pd content: 60% by weight) as noble metal precursors. A calculated amount of noble metal precursor was dispersed in a 250 mL round-bottom flask containing 2 g calcined NaMOR zeolite dispersed in 150 mL deionized water (with a final ratio of ~3 wt.% noble metals to MOR). The resultant mixture was stirred overnight (~12 h) under ambient conditions. Subsequently, the solution mixture was filtered/centrifuged, washed with deionized water, dried at 100 °C overnight, and calcined in air at 450 °C for 4 h. A similar procedure was adopted for the synthesis of the RuMOR, RhMOR, and PdMOR catalysts.

3.2.3. Characterization of Catalysts

Powder XRD patterns were recorded on a PANalytical Empyrean X-ray diffractometer (Almelo, Netherlands) equipped with Cu-Kα radiation (40 kV, 30 mA) at a rate of 7.5° min^{-1} over the 2θ range of 5 to 55°. SEM images were recorded on an Analytical UHR Schottky emission scanning electron Hitachi SU-70 microscope (Tokyo, Japan). The SEM samples (in powder form) were prepared on carbon tape, and later the platinum spin coating of each sample was done for 100 s. The SEM analysis for all the samples was carried out at the accelerating voltage of 15.0 kV. TEM images of the catalysts were obtained by using a Tecnai F-20 (Philips) instrument (OR, USA) operating at 200 kV (lattice resolution: 0.19 nm). Images were recorded with a charged coupled device (CCD) camera (CA, USA) at high magnification under low-dose conditions. All the TEM samples were prepared by dispersing the catalyst powder in ethyl alcohol under ultrasonication. A few droplets of suspension were kept on a carbon-coated copper grid and allowed to dry under ambient conditions. Elemental mapping was carried out by energy dispersive spectroscopy (EDAX STD-S PV7747/67, MA, USA) with an energy resolution of 129 eV. X-ray photoelectron spectroscopy was performed on a high-performance Thermo Scientific (HP-XPS) K-ALPHA$^+$ instrument (MA, USA) with an ultimate vacuum of 5×10^{-9} mbar pressure (pass energy of 200 eV for survey spectra and 50 eV for narrow spectra, take-off angle of 60°) equipped with a monochromated Al-Kα source connected to a 128-channel detector. Thermogravimetric analysis (TGA) of the catalysts was performed in the temperature range of 50 to 900 °C at the ramping rate of 10 °C min^{-1} under N_2 atmosphere (20 mL min^{-1}) on a Perkin Elmer STA 6000 (simultaneous thermal analyser, MA, USA) instrument. Solid-state MAS ^{27}Al NMR data were obtained at a spinning rate of 10 kHz on a JEOL ECZ400R instrument (Tokyo, Japan). For each analysis, a total 2048 number of scans were performed (with the relaxation delay of 1 s) using a standard of 1.1 M $Al(NO_3)_3$ in D_2O. The surface area of all the materials was determined by applying the BET equation to the isothermal N_2 adsorption data acquired at 77 K using a BEL/Besorp mini II instrument (Tokyo, Japan). Prior to the measurements, all the samples were degassed at 400 °C for 2 h. Elemental analysis was carried out with a Thermo Scientific iCAP 6300 DuO ICP-OES instrument equipped with a charge injection device (CID) detector (MA, USA) working in the wavelength range of 166 to 841 nm. The data were obtained at wavelengths of 396.1, 212.4, 340.4, 240.2, and 343.4 nm for Al, Si, Pd, Ru, and Rh, respectively.

3.2.4. Catalytic Transfer Hydrogenolysis (CTH) of Glycerol to 2-Isopropoxy-Propan-1-Ol

CTH reactions were performed in a 50 mL stainless-steel autoclave high pressure liquid batch reactor (Korea) equipped with a pressure regulator, under N_2 atmosphere. In a typical reaction, 0.4 g of freshly prepared catalyst (NaMOR(cal), RuMOR(cal), PdMOR(cal), or RhMOR(cal)) was charged into an autoclave containing 9 g isopropyl alcohol (propan-2-ol). To this mixture, 0.5 g (5.43 mmol) of glycerol was added. The resultant mixture was thoroughly purged twice with N_2 to remove residual gases and moisture inside the vessel, and an initial N_2 pressure of 0.5 MPa was applied for each reaction. The reactor was then heated to 140 °C and stirred at 500 rpm for 72 h. The reactor was autogenously pressurized to 1.4 MPa under the aforementioned reaction conditions. After a designated

time, the reaction was stopped, and the reactor was cooled to ambient temperature. An internal standard (dodecane) was added to the reaction solution. The solid catalyst was filtered out by using a syringe filter (pore size 0.22 μm), and the liquid part of the reaction mixture was analyzed by gas chromatography (6500 GC, Younglin instrument, Gyeonggi-do, Korea) with a DB-5 column and a flame ionization detector (FID, CA, USA).

3.2.5. Product Analysis

The reaction solution and products were analyzed and identified by GC, GC-MS, and ^{1}H NMR. The compounds were first analysed by GC (6500 GC, YL instrument, Gyeonggi-do, Korea) equipped with a DB-5 column (30 m × 0.32 mm × 1.50 μm) and a flame ionization detector (FID, CA, USA). GCMS analysis was performed on an Agilent Technologies 5975B Inter XL MSD instrument equipped with an Agilent J&W GC column (30 m × 0.32 mm × 0.25 μm) and mass selective detector (MSD, CA, USA). ^{1}H NMR analysis was carried out with an Agilent ProPulse 500 MHz NMR spectrometer (CA, USA). The NMR samples were prepared in deuterated methanol (CD_3OD). The catalytic performance was calculated in terms of the conversion (%). The reaction between glycerol and propan-2-ol was confirmed from the GC, GCMS, and ^{1}H NMR data. The % conversion was calculated based on the glycerol concentration in the reaction mixture before and after the reaction. The product selectivity was confirmed from the GC and GCMS data, where only one additional peak (apart from those of the reactants) was observed after the reaction.

$$\% \text{ Conversion } = \frac{\text{mole of converted glycerol}}{\text{mole of initial glycerol}} \times 100$$

4. Conclusions

In summary, we have reported a novel approach for catalytic application of mono-metallic noble metal ion-exchanged MOR zeolites for the selective CTH conversion of glycerol to 2-isopropoxy-propan-1-ol in the presence of propan-2-ol under mild reaction conditions, in the absence of external hydrogen. The synthesized noble metal-based catalysts (RuMOR, RhMOR, and PdMOR) were characterized via XRD, SEM, TEM, XPS, TGA, solid-state ^{27}Al MAS NMR, and a BET surface area analyzer, which affirms the synthesis of highly stable materials. This study, for the first time, proposes an alternative use of glycerol to obtain 2-isopropoxy-propan-1-ol by controlling the reaction conditions with 100% product selectivity, and confirms that the ruthenium-based ion-exchanged mordenit (RuMOR) displayed best catalytic performance compared to the other catalysts. As part of future research, the effects of other catalytic parameters and reaction conditions are currently under investigation. The obtained product is highly applicable as an effective solvent for resin, dyes, and use in surface coating.

Supplementary Materials: The following are available online at http://www.mdpi.com/2073-4344/9/11/885/s1, Figure S1: Schematic representation of catalytic transfer hydrogenolysis (CTH) conversion of glycerol to 2-isopropoxy-propan-1-ol in the presence of propan-2-ol over noble metal ion-exchanged mordenite (XMOR, where X denotes noble metals; Ru, Rh, and Pd), Figure S2: GCMS spectrum of 2-isopropoxy-propan-1-ol (MW = 118.17) obtained after CTH conversion of glycerol in the presence of propan-2-ol over XMOR (X= Ru, Pd, and Rh), Figure S3: ^{1}H NMR spectrum of resultant solution after CTH reaction of glycerol in the presence of propan-2-ol (the spectra were obtained in deuterated methanol), Figure S4: ^{1}H NMR spectra of the starting reaction mixture (glycerol, propan-2-ol), Table S1: Properties of NaMOR(cal), RuMOR(cal), RhMOR(cal) and PdMOR(cal) catalysts.

Author Contributions: Conceptualization and methodology, B.K.S. and K.N.; data investigation and writing—original draft preparation, B.K.S.; discussion, writing—review and editing, B.K.S., Y.K., S.K., and K.N.; supervision, K.N.

Funding: This work was supported by a National Research Foundation of Korea (NRF) grant, funded by the Korean Government (MSIT) (NRF-2015R1A4A1041036 & NRF-2018R1C1B6006076).

Acknowledgments: The solid-state MAS ^{27}Al NMR spectra were obtained at the Korea Basic Science Institute, Gwangju Branch.

Conflicts of Interest: The authors declare no conflict of interest.

References

1. Maurielloa, F.; Ariga, H.; Musolino, M.G.; Pietropaolo, R.; Takakusagi, S.; Asakura, K. Exploring the catalytic properties of supported palladium catalysts in the transfer hydrogenolysis of glycerol. *Appl. Catal. B Environ.* **2015**, *166*, 121–131. [CrossRef]
2. Samudrala, S.P.; Kandasamy, S.; Bhattacharya, S. Turning Biodiesel Waste Glycerol into 1,3-Propanediol: Catalytic Performance of Sulphuric acid-Activated Montmorillonite Supported Platinum Catalysts in Glycerol Hydrogenolysis. *Sci. Rep.* **2018**, *8*, 7484. [CrossRef] [PubMed]
3. Quispe, C.A.G.; Coronado, C.J.R.; Carvalho, J.A. Glycerol: Production, consumption, prices, characterization and new trends in combustion. *Renew. Sustain. Energy Rev.* **2013**, *27*, 475–493. [CrossRef]
4. Pagliaro, M.; Ciriminna, R.; Kimura, H.; Rossi, M.; Pina, C.D. From glycerol to value-added products. *Angew. Chem. Int. Ed.* **2007**, *46*, 4434–4440. [CrossRef]
5. Gandarias, I.; Arias, P.L.; Fernández, S.G.; Requies, J.; Doukkali, M.E.; Güemez, M.B. Hydrogenolysis through catalytic transfer hydrogenation: Glycerol conversion to 1,2-propanediol. *Catal. Today* **2012**, *195*, 22–31. [CrossRef]
6. Miyazawa, T.; Kusunoki, Y.; Kunimori, K.; Tomishige, K. Glycerol conversion in the aqueous solution under hydrogen over Ru/C plus an ion-exchange resin and its reaction mechanism. *J. Catal.* **2006**, *240*, 213–221. [CrossRef]
7. Bagheri, S.; Julkaplin, N.M.; Yehye, W.A. Catalytic conversion of biodiesel derived raw glycerol to value added products. *Renew. Sustain. Energy Rev.* **2015**, *41*, 113–127. [CrossRef]
8. Vasiliadou, E.S.; Heracleous, E.; Vasalos, I.A.; Lemonidou, A.A. Ru-based catalysts for glycerol hydrogenolysis—Effect of support and metal precursor. *Appl. Catal. B Environ.* **2009**, *92*, 90–99. [CrossRef]
9. Nakagawa, Y.; Tomishige, K. Heterogeneous catalysis of the glycerol hydrogenolysis. *Catal. Sci. Technol.* **2011**, *1*, 179–190. [CrossRef]
10. Zhou, C.H.; Beltramini, J.N.; Fan, Y.X.; Lu, G.Q. Chemoselective catalytic conversion of glycerol as a biorenewable source to valuable commodity chemicals. *Chem. Soc. Rev.* **2008**, *37*, 527–549. [CrossRef]
11. Chheda, J.N.; Huber, G.W.; Dumesic, J.A. Liquid-phase catalytic processing of biomass-derived oxygenated hydrocarbons to fuels and chemicals. *Angew. Chem. Int. Ed.* **2007**, *46*, 7164–7183. [CrossRef] [PubMed]
12. Luo, W.T.; Yu, Y.L.; Gong, L.F.; Du, H.; Jiang, M.; Ding, Y.J. The influence of impregnation sequence on glycerol hydrogenolysis over iridium-rhenium catalyst. *React. Kinet. Mech. Catal.* **2016**, *118*, 481–496. [CrossRef]
13. Balaraju, M.; Jagadeeswaraiah, K.; Prasad, P.S.S.; Lingaiah, N. Catalytic hydrogenolysis of biodiesel derived glycerol to 1,2-propanediol over Cu–MgO catalysts. *Catal. Sci. Technol.* **2012**, *2*, 1967–1976. [CrossRef]
14. Pudi, S.M.; Biswas, P.; Kumar, S. Selective hydrogenolysis of glycerol to 1,2-propanediol over highly active copper-magnesia catalysts: Reaction parameter, catalyst stability and mechanism study. *J. Chem. Technol. Biotechnol.* **2015**, *91*, 2063–2075. [CrossRef]
15. Barbelli, M.L.; Santori, G.F.; Nichio, N.N. Aqueous phase hydrogenolysis of glycerol to bio-propylene glycol over Pt–Sn catalysts. *Bioresour. Technol.* **2012**, *111*, 500–503. [CrossRef]
16. Musolino, M.G.; Scarpino, L.A.; Mauriello, F.; Pietropaolo, R. Selective transfer hydrogenolysis of glycerol promoted by palladiumcatalysts in absence of hydrogen. *Green Chem.* **2009**, *11*, 1511–1513. [CrossRef]
17. Cortright, R.D.; Davda, R.R.; Dumesic, J.A. Hydrogen from catalytic reforming of biomass-derived hydrocarbons in liquid water. *Nature* **2002**, *418*, 964–967. [CrossRef]
18. Wang, J.; Zhao, X.C.; Lei, N.; Li, L.; Zhang, L.L.; Xu, S.T.; Miao, S.; Pan, X.L.; Wang, A.Q.; Zhang, T. Hydrogenolysis of Glycerol to 1,3-propanediol under Low Hydrogen Pressure over WO_x-Supported Single/Pseudo-Single Atom Pt Catalyst. *ChemSusChem* **2016**, *9*, 784–790. [CrossRef]
19. Zhoua, C.H.; Deng, K.; Serio, M.D.; Xia, S.; Tonga, D.S.; Li, L.; Lin, C.X.; Beltramini, J.; Zhang, H.; Yu, W.H. Cleaner hydrothermal hydrogenolysis of glycerol to 1,2-propanediol over Cu/oxide catalysts without addition of external hydrogen. *Mol. Catal.* **2017**, *432*, 274–284. [CrossRef]

20. Singh, B.K.; Kim, Y.; Baek, S.B.; Meena, A.; Sultan, S.; Kwak, J.H.; Kim, K.S. Template free facile synthesis of mesoporous mordenite for bulky molecular catalytic reactions. *J. Ind. Eng. Chem.* **2018**, *57*, 363–369. [CrossRef]
21. Zhang, T.; Ge, Y.; Wang, X.; Chen, J.; Huang, X.; Liao, Y. Polymeric Ruthenium Porphyrin-Functionalized Carbon Nanotubes and Graphene for Levulinic Ester Transformations into γ-Valerolactone and Pyrrolidone Derivatives. *ACS Omega* **2017**, *2*, 3228–3240. [CrossRef] [PubMed]
22. Chakroune, N.; Viau, G.; Ammar, S.; Poul, L.; Veautier, D.; Chehimi, M.M.; Mangeney, C.; Villain, F.; Fievet, F. Acetate- and Thiol-Capped Monodisperse Ruthenium Nanoparticles: XPS, XAS, and HRTEM Studies. *Langmuir* **2005**, *21*, 6788–6796. [CrossRef] [PubMed]
23. Yuan, Q.; Zhang, D.; Haandel, L.V.; Ye, F.; Xue, T.; Hensen, E.J.M.; Guan, Y. Selective liquid phase hydrogenation of furfural to furfuryl alcohol by Ru/Zr-MOFs. *J. Mol. Catal. A Chem.* **2015**, *406*, 58–64. [CrossRef]
24. Sunol, J.J.; Bonneau, M.E.; Roue, L.; Guay, D.; Schulz, R. XPS surface study of nanocrystalline Ti–Ru–Fe materials. *Appl. Surf. Sci.* **2000**, *158*, 252–262. [CrossRef]
25. Groves, J.T.; Quinn, R. Models of oxidized heme proteins. Preparation and characterization of a trans-dioxoruthenium(VI) porphyrin complex. *Inorg. Chem.* **1984**, *23*, 3844–3846. [CrossRef]
26. Yamamoto, Y.; Matsuzaki, T.; Tanaka, S.; Nishihira, K.; Ohdan, K.; Nakamura, A.; Okamoto, Y. Catalysis and characterization of Pd/NaY for dimethyl carbonate synthesis from methyl nitrite and CO. *J. Chem. Soc. Faraday Trans.* **1997**, *93*, 3721–3727. [CrossRef]
27. Suarez, S.; Yates, M.; Petre, A.L.; Martín, J.A.; Avila, P.; Blanco, J. Development of a new Rh/TiO_2–sepiolite monolithic catalyst for N_2O decomposition. *Appl. Catal. B Environ.* **2006**, *64*, 302–311. [CrossRef]
28. Larichev, Y.V.; Netskina, O.V.; Komova, O.V.; Simagina, V.I. Comparative XPS study of Rh/Al_2O_3 and Rh/TiO_2 as catalysts for $NaBH_4$ hydrolysis. *Int. J. Hydrogen Energy* **2010**, *35*, 6501–6507. [CrossRef]
29. Wang, M.; Zhong, J.Q.; Kestell, J.; Waluyo, I.; Stacchiola, D.J.; Boscoboinik, J.A.; Lu, D. Energy Level Shifts at the Silica/Ru(0001) Heterojunction Driven by Surface and Interface Dipoles. *Top. Catal.* **2017**, *60*, 481–491. [CrossRef]
30. Kuroda, Y.; Kotani, A.; Maeda, H.; Moriwaki, H.; Morimat, T. The State of Excessively Ion-exchanged Copper in Mordenite: Formation of Tetragonal Hydroxy-bridged Copper Ion. *J. Chem. Soc. Faraday Trans.* **1992**, *88*, 1583–1590. [CrossRef]
31. Dyballa, M.; Pappas, D.K.; Kvande, K.; Borfecchia, E.; Arstad, B.; Beato, P.; Olsbye, U.; Svelle, S. On How Copper Mordenite Properties Govern the Framework Stability and Activity in the Methane-to-Methanol Conversion. *ACS Catal.* **2019**, *9*, 365–375. [CrossRef]
32. Mennicke, W. 1:2 Chromium Complex Dyestuffs. U.S. Patent 5,484,900, 16 January 1996.
33. Knifton, J.F. Synthesis of Low Molecular Weight Ethylene Propylene Glycol Ethers via Olefin Addition to the Corresponding Glycol. Europe Patent EP0,419,077A2, 27 March 1991.